MULTISCALE MODEL. SIMUL.
Vol. 19, No. 3, pp. 1143–1166

HOW DO DEGENERATE MOBILITIES DETERMINE SINGULARITY FORMATION IN CAHN–HILLIARD EQUATIONS?*

CATALINA PESCE† AND ANDREAS MUENCH†

Abstract. Cahn–Hilliard models are central for describing the evolution of interfaces in phase separation processes and free boundary problems. In general, they have nonconstant and often degenerate mobilities. However, in the latter case, the spontaneous appearance of points of vanishing mobility and their impact on the solution are not well understood. In this paper we develop a singular perturbation theory to identify a range of degeneracies for which the solution of the Cahn–Hilliard equation forms a singularity in infinite time. This analysis forms the basis for a rigorous sharp interface theory and enables the systematic development of robust numerical methods for this family of model equations.

Key words. phase-field models, sharp interface, lubrication theory, degenerate fourth order partial differential equations, matched asymptotic expansions

AMS subject classifications. 35A21, 35B40, 35G20, 74N20, 76M45, 82C26

DOI. 10.1137/21M1391249

1. Introduction.

Since its introduction [23, 20, 21, 24], the Cahn–Hilliard equation and its many variations have become fundamental tools for describing the separation of phases over a large range of time and space scales in many applications. In the most basic case of two partially miscible materials, such as binary alloys or polymeric liquids, this includes the early onset of the phase separation from a homogeneous, unstable state via spinodal decomposition [20, 21] and subsequent nonlinear evolution at later stages where coarsening occurs [41, 67] until the quasi-stationary stages where only few, large, and almost homogeneous domains remain. Due also to its ability to allow for topological changes of the domain, phase-field models based on extensions of the Cahn–Hilliard equation are frequently used as the basis for numerical simulations of, for example, the evolution of interfaces between immiscible liquids. These applications exploit the fact that in a phase-field model, the interfaces are represented by a thin layer over which the order parameter varies rapidly but continuously. Examples of such processes are surface diffusion and electromigration in crystals and alloys [25, 70, 22, 37, 17, 8, 9], motion of immiscible fluids with free boundaries [36, 1, 46, 19, 69], polymer blends [57, 35, 26], tumor growth models [29, 62, 54], and lithiation in battery electrodes [58], to name just a few.

Stated in the form introduced by [23, 24], the Cahn–Hilliard equation can be written as

$$u_t = -\nabla \cdot \mathbf{j}, \qquad \mathbf{j} = -M(u)\nabla\mu, \qquad \mu = -\varepsilon^2\nabla^2 u + f'(u), \tag{1.1a}$$

with the (conserved) order parameter u, such that $|u| \leq 1$ and $\varepsilon > 0$. The homogeneous free energy and mobility are, respectively,

*Received by the editors January 11, 2021; accepted for publication (in revised form) April 26, 2021; published electronically July 13, 2021.
https://doi.org/10.1137/21M1391249
Funding: This work was supported by the EPSRC Centre for Doctoral Training in Partial Differential Equations: Analysis and Applications through EPSRC grant EP/L015811/1. The first author acknowledges support from the Chilean National Agency for Research and Development (ANID) through the Scholarship Program DOCTORADO BECAS CHILE/2018 - 72190029.
†Mathematical Institute, University of Oxford, Oxford, OX2 6GG, UK (pesce@maths.ox.ac.uk, muench@maths.ox.ac.uk).

(1.1b)
$$f(u) = (\theta/2)\,[(1-u)\ln(1-u) + (1+u)\ln(1+u)] + (1-u^2)/2, \qquad M(u) = 1-u^2,$$

where $\theta \geq 0$ denotes a normalized temperature. For $0 < \theta < 1$ the free energy in (1.1b) has two distinct minima $u_\pm$ and the system separates into two phases with those relative concentration values. The diffuse interface layers between these phases domains are thin if ε is small. The term Cahn–Hilliard is often used more broadly to describe a class of phase-field models that have the general form (1.1) but different free energies and mobilities, for example, a quartic polynomial with fixed minima $u = \pm 1$, such as

$$f(u) = \frac{1}{2}(1-u^2)^2, \tag{1.2}$$

and a constant mobility $M(u) \equiv 1$.

While a different mobility does not change the energy landscape, it does strongly affect the kinetics of the process. For constant mobility, the flux depends only on the gradient of the chemical potential μ and the diffusive flux $\mathbf{j}$ can freely transport material through the bulk in the direction of decreasing μ. The kinetics become clearer when one takes ε, and thus the interface width, to 0. For the constant mobility Cahn–Hilliard equation, Pego [63] showed, via matched asymptotics, that the sharp interface limit is the Mullins–Sekerka problem, which inspired the rigorous proof by Alikakos, Bates, and Chen [3]. The Mullins–Sekerka problem couples the interface motion to the bulk diffusion between the domains at the late stages of the coarsening process.

In contrast, nonlinear mobilities that degenerate at or near the minima of the free energy suppress bulk diffusion, so that transport along the interface, i.e., surface diffusion, becomes more important. Using asymptotic methods, Cahn and Taylor [25] demonstrated that for $\theta \ll 1$ and for a double-obstacle free energy ($\theta = 0$), the sharp interface limit for (1.1) is simply the surface diffusion equation, with no transport across the bulk, at least to leading order. On the other hand, for the case of a quartic free energy ((1.1a) and (1.2)), the degenerate mobility leads to a subtle balance between bulk and surface diffusion, so that to leading order, both enter the sharp interface limit [31, 53]. This has come as a surprise to some in the community, as by routine application of Pego's asymptotic approach, one can easily miss the contribution from bulk diffusion and obtain the wrong sharp interface model [51, 52, 76]. The correct and consistent evaluation of the flux requires the use of exponential matching [53].

The results in [51, 53, 52] highlight the subtleties arising from degenerate mobilities and the importance of investigating the equations carefully. Besides the derivation of the sharp interface limit in [53], another aspect became apparent upon solving the axisymmetric PDE on a circular, two-dimensional domain with initial data u_0 strictly bounded between -1 and $+1$. This represents a situation where the phases have separated into two domains, a disc centered at the origin with a composition close to one phase, surrounded by an annular region with a composition near the opposite phase, and a diffuse interface between them. As a numerical result in [53] reveals, the solution evolves so that near the interface, $|u|$ develops a maximum that quickly approaches 1, that is, the value for which the mobility degenerates.

This phenomenon is intimately connected with a property of stationary solutions to Cahn–Hilliard equations with smooth polynomial free energies. These are well-studied and, in particular, existence and uniqueness of small energy stationary solutions have been proven in Niethammer [60] using a rigorous matched asymptotics

expansion technique that also captures the qualitative features of the solution. Nontheless the following property (referred to as the Gibbs-Thompson effect in [31]) has often been overlooked: In the presence of curved interface layers between phases, the chemical potential is non-zero in equilibrium, and the "outer" solution i.e. the solution away from interface layers, differs from the minima of the free energy by a small amount proportional to the curvature. Inside convex domains, the value is in fact outside of the interval delineated by the minima of the free energy (i.e. here ± 1). Since time dependent solutions of Cahn–Hilliard equations monotonically decrease their energy, they are expected to converge to stationary solutions; in particular, to the one investigated by Niethammer [60]. As a result, u must approach ± 1 somewhere, thus forcing the degenerate mobility $M(u)$ in (1.1b) to become zero.

This observation raises interesting questions that have important implications for established practices. To begin with, is $u = \pm 1$ achieved in finite or infinite time? What determines this? Since at those points mobilities like (1.1b) degenerate, does it depend on how degenerate M is? We note that some authors [56, 66, 71, 72, 73, 78] choose a low-degeneracy mobility with a degree of two, that is, the square of the form used in (1.1b), but higher degeneracies can also be useful to understand the full spectrum of the solution's behavior. Next, what happens, for example, in the case that $|u|$ approaches 1 (and hence $M(u)$ approaches 0) in finite time? Can this lead to loss of regularity and, thus, to singularity formation? Will the vanishing mobility freeze the solution there and prevent the set $\{M(u) = 0\}$ from moving, and how will that influence the evolution of the diffuse interface and hence the sharp interface limit? How will that affect long-time pattern formation in numerical simulations?

An early paper by Elliott and Garcke [38], where they proved existence of solutions for a class of degenerate Cahn–Hilliard models, first raised the question of how the set $\{M(u) = 0\}$ evolves. In fact, pinning was observed in numerical solutions of degenerate Allen–Cahn/Cahn–Hilliard systems [6], in contrast to the constant mobility case. Moreover, solutions with a waiting time behavior are also conceivable [61]. Numerical experiments in [7] demonstrate that the choice of the relative magnitudes of the mesh and the temporal step size yields at least two solutions with very different behavior. If the mesh sizes are taken to zero much faster than the step size, the solution the scheme converges to is pinned at the boundary of the set $\{M(u) = 0\}$ and hence it is stationary, while another, moving, solution emerges if the step and mesh sizes are in a distinguished limit with each other. Such a behavior is important to know and understand, as selecting and changing step and mesh sizes is standard practice in numerical simulations, and in fact is often done automatically as part of the adaptivity implemented in ready-to-run simulation packages. These results highlight the role of nonuniqueness of solutions, which also prompts questions about the implications for the sharp interface limit, in particular, can different solutions have different sharp interface limits? As a consequence, it becomes essential to investigate the situation at points $\{M(u) = 0\}$, which are typically points where the solution becomes singular, in the sense that the regularity is reduced [27], requiring the introduction of weak solution concepts [38, 11].

These questions overlap with another important class of fourth order PDEs with degenerate mobility, namely the surface tension driven thin film model. The thin film equation for surface tension driven flows (and its variants) has a rich history and a huge literature covering questions (1) on the formation and evolution of sets where the mobility is zero [27, 28, 14, 11, 15, 12, 74, 75, 77, 39, 65, 64, 59], especially in the context of the fundamental questions in fluid mechanics about the moving three-phase contact-line (see, e.g., [43, 5, 50, 45], and see also [13]), and (2) on the impact

of the degree of degeneracy on the solutions [4, 49]. In a situation where sufficient pressure is applied to the boundary of a thin film, singularities are always forced. In particular, questions about how the thin film height goes to zero and if the singularity occurs in finite or infinite time have been discussed in the literature [27, 28, 14]. The connection between thin films and degenerate Cahn–Hilliard problems offers a lot of potential, and even though it has been highlighted earlier [48, 61], it has rarely been directly exploited. Furthermore, in this paper, the asymptotic techniques from the thin film literature have proven to be fundamental for understanding the behavior of a degenerate Cahn–Hilliard problem.

We will focus on polynomial double well potentials which have their minima aligned with the zeros of the degenerate mobilities. The vast majority of numerical simulations in practical applications use this combination rather than a logarithmic free energy (1.1b), for example in tumor growth models [29, 62, 54], in diffusive models of interfaces in fluid flow problems [42, 55, 36], and also for surface diffusion in materials [56, 66, 71, 72, 73, 78]. It is therefore important to develop a thorough understanding for models with this combination and their sharp interface limits, on which, for example in the case of surface diffusion, the physical justification hinges. Above we have given an overview of the intricacies that arise for these models, and an example where a lack of clear understanding has led to an erroneous sharp interface limit. Degenerate mobilities combined with the logarithmic free energy (which is directly motivated by statistical mechanics) also need to be explored beyond what is known from classical references, e.g., [22], regarding regions where the mobility becomes small or zero, but this requires a separate investigation that is part of ongoing work.

We will also consider the solution on a particular domain, namely on a two-dimensional axially symmetric domain with a quartic polynomial free energy f and a mobility M which vanishes at the minima of f, and where the degree of degeneracy is treated as a parameter $n \in \mathbb{R}_+$. We show that the solution develops points where $|u| \to 1$, which can form in either finite or infinite time, and that for a range of mobilities, there are attracting solutions that belong to the latter category. These solutions are analyzed by singular perturbation methods.

Summarizing, we find the following picture for the long-time asymptotic solution to the specific degenerate Cahn–Hilliard problem we consider here, depending on the degree of degeneracy n of the mobility. For $n > 2$, we obtain an infinite-time solution consisting of three spatial regimes: the annular region where the solution is quasi-stationary, a touchdown region where the fastest approach to zero in the mobility occurs, and the central region near the center of the disc. Three subcases ($2 < n < 3$, $n = 3$, $3 < n$) occur because the higher order terms in the expansions for the solution in these subregions change, i.e., the matching to leading order is not affected. For $n \leq 2$, the leading order term in these expansions changes, signaling a transition into a new asymptotic state. Preliminary investigations suggest that a solution with infinite time touchdown exists for $1/2 < n < 2$ and for $n = 2$, with different scalings than the one for $n > 2$. Determining the asymptotic solution for $n \leq 2$ is part of ongoing work.

The layout of the paper is as follows. In section 2, we summarize the precise statement of the axially symmetric Cahn–Hilliard equation that we consider. In section 3, we present the result of numerical solutions for a range of values n for the degree of degeneracy of M. In particular, we determine the self-similar regions that develop in the long-time solution for the example of $n = 4$. In section 4, we systematically derive an asymptotic approximation for the long-time behavior of this solution for the case

$n > 2$ using matched asymptotics. In section 5, we discuss our results and point to possible further questions and avenues of research.

2. Problem statement. We take (1.1a) on the two-dimensional unitary ball for a radially symmetric smooth function $u = u(r, t)$, which written in polar coordinates corresponds to

$$u_t = -\frac{1}{r}\frac{\partial(rj)}{\partial r}, \qquad j = -M(u)\frac{\partial \mu}{\partial r}, \qquad \mu = -\frac{\varepsilon^2}{r}\frac{\partial}{\partial r}\left(r\frac{\partial u}{\partial r}\right) + f'(u), \tag{2.1a}$$

for $0 < r < 1$ and $t > 0$. We also assume that u and its derivatives with respect to Cartesian coordinates are continuous at the origin, which implies the boundary conditions

$$\partial_r u = 0, \qquad \partial_{rrr} u = 0, \qquad \text{at } r = 0, \tag{2.1b}$$

and moreover, we assume that we have a neutral surface at $r = 1$ and no flux, so that

$$\partial_r u = 0, \quad j = 0, \qquad \text{at } r = 1. \tag{2.1c}$$

We also need to prescribe an initial condition

$$u(r, 0) = u_{\text{init}}(r), \tag{2.1d}$$

which we specify further in the next section. Typically, it will be a scaled tanh-profile that is strictly bounded between $+1$ and -1. The homogeneous free energy is given by a double-well potential

$$f(u) = \frac{1}{2}(1 - u^2)^2, \tag{2.1e}$$

and the mobility by

$$M(u) = (1 - u^2)^n, \tag{2.1f}$$

where $n > 0$ is a real parameter. Common values for this parameter are $n = 1$, 2. They are used in models for surface diffusion [56, 66, 71, 72, 73, 78], tumor growth [29, 62, 54], and the motion of interfaces in fluid flow [42, 55, 36]. However, in thin film flow, conducting a systematic study that allows the degree of degeneracy n to vary continuously over a large range of (even negative) values has proved to be a very fruitful approach. In particular, large n often have solutions with the simpler structure from which it is then easier to expand the study to smaller n by identifying the values where, for example, an asymptotic regime ceases to be valid [18, 49, 14]. We therefore adopt this approach here, too, and focus in this paper on $n > 2$. Moreover, regularizations of low-degenerate mobilities that increase the mobility to large n are very useful for selecting nonnegative solutions of (2.1), especially when combined with a positivity preserving numerical scheme [79].

The mobility in (2.1f) is the form that we shall use most often in this paper, though we also discuss two variants, in particular where we refer to results in the literature. One variant, considered, for example, by Elliott and Garcke [38], is to truncate the mobility, so that

$$M(u) = (1 - u^2)_+^n, \tag{2.2}$$

where the subscript + denotes the positive part of the expression (taken before the expression is raised to the power of n). A second variant, used by Dai and Du [31, 32, 33], is to take instead the absolute value,

$$M(u) = |1 - u^2|^n. \tag{2.3}$$

In all cases, the parameter $n > 0$ determines the degree of degeneracy of the mobility. These variants differ for values of u with $|u| > 1$, where (2.1f) becomes undefined for noninteger n or changes sign for odd n, leading to ill-posedness unless n is even. We avoid these situations in the current article by focusing on bounded solutions $|u| \leq 1$.

3. Numerical solution. We begin by inspecting numerical solutions of (2.1) for three different groups of the mobility: (a) constant mobility, $M = 1$, corresponding to (2.1f) with $n = 0$; (b) degenerate mobility with $n = 1$; (c) degenerate mobility with $n = 4$. The initial data is given by (2.1d), with

$$u_{\text{init}}(r) = -0.95 \tanh\left(\frac{r - 0.5}{\varepsilon}\right). \tag{3.1}$$

Such tanh-like profiles are a common choice for numerical simulations where phase-field models are used to track the evolution of a free interface, or to capture the late stages of a phase separation process; see [72], [71]. Unless otherwise stated, we choose

$$\varepsilon = 0.1. \tag{3.2}$$

Notice the initial profile above satisfies the boundary conditions (2.1b), (2.1c) except for exponentially small terms. Replacing (3.1) in the vicinity of $r = 0$ and $r = 1$ by constant values $+1$ and -1, respectively, so that the initial profile satisfies the boundary conditions, did not change the numerical results in any noticeable way.

The numerical solutions for (2.1) with initial data (3.1) presented here were obtained by a finite difference code using centered differences in space and and implicit Euler scheme in time. The spatial grid was equidistant, and we used a step doubling scheme to control the error in time.

Constant mobility. We see in Figure 1, left, that the solution develops a maximum at a radius $\bar{r}(t)$ near $r = 0.15$, which quickly crosses $u = 1$ at $t = t_* = 0.0106$, after which u settles into a stationary solution. To understand better the intuition behind the long-time solution of the constant mobility case we need to introduce the free energy associated with this system, which, in polar coordinates, is given by

$$\mathcal{F}[u] = \int_0^1 \left[\frac{\varepsilon^2}{2}(\partial_r u)^2 + f(u)\right] r \mathrm{d}r. \tag{3.3}$$

This energy is always nonincreasing along a solution trajectory, i.e., if $u(t)$ is a solution of (2.1a), (2.1c), then $E(t) := \mathcal{F}[u(t)]$ satisfies

$$\frac{\mathrm{d}E}{\mathrm{d}t} = -\int_0^1 M(u)\,(\partial_r \mu)^2\, r \mathrm{d}r \leq 0. \tag{3.4}$$

Since $E \geq 0$, this means that $E \to E_\infty$ as $t \to \infty$, and $\mathrm{d}E/\mathrm{d}t \to 0$. (Notice this is true also for general nonlinear mobilities provided they are nonnegative.) Since M is constant, μ converges to a constant, say, μ_c. If the solution converges to a stationary solution $U(r)$ of (2.1), which is known to be true at least for the case of constant mobility with logarithmic [2] or quartic polynomial homogeneous free energy [68], then $U(r)$ must satisfy

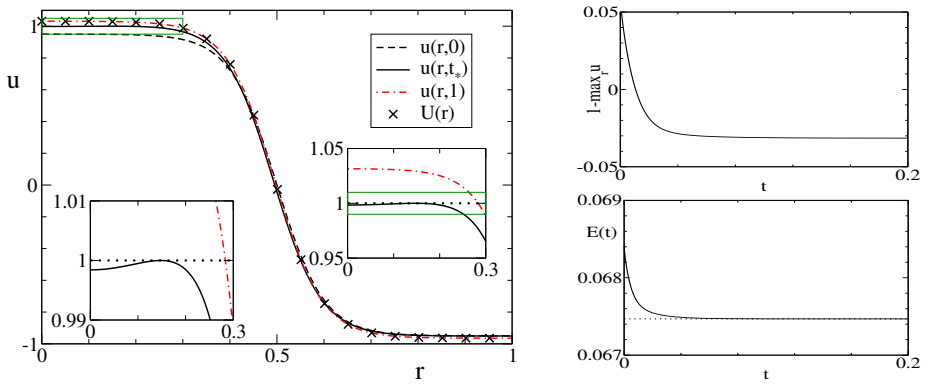

FIG. 1. *Left: Solution u of (2.1) with constant mobility $M = 1$, at different times $t = 0$, $t = t_* = 1.06 \times 10^{-2}$, $t = 1$. This is compared with the stationary solution $U(r)$, which satisfies (3.5) and (3.7). The right inset shows a zoom of the area delineated by a thin solid box, and the left inset in turn zooms into the area between the horizontal vertical lines in the first inset. A thin dotted line at $u = 1$ has been added to both insets for guidance. Right: Top, evolution of $1 - \max_r u(r,t)$, and bottom, of the energy $E(t)$ of the solution. The thin dotted line shows the energy for the stationary solution of (3.5), (3.7).*

$$-\frac{\varepsilon^2}{r}\frac{\mathrm{d}}{\mathrm{d}r}\left(r\frac{\mathrm{d}U}{\mathrm{d}r}\right) + f'(U) = \mu_c, \tag{3.5a}$$

$$U'(1) = 0, \tag{3.5b}$$

$$U'(0) = 0. \tag{3.5c}$$

The additional degree of freedom μ_c is used to accommodate a mass constraint that the solution inherits from the initial condition. The system (2.1), (2.1b), (2.1c) conserves mass, that is, for

$$m(t) := \int_0^1 u(r,t) r \mathrm{d}r \tag{3.6}$$

one easily finds that $\mathrm{d}m/\mathrm{d}t = 0$ along a solution $u(r,t)$; therefore, for the stationary solution, we need to enforce

$$\int_0^1 U(r) r \mathrm{d}r = m_0, \tag{3.7}$$

where

$$m_0 = \int_0^1 u_{\mathrm{init}}(r) r dr. \tag{3.8}$$

It has been shown in [60] that for any initial mass m_0, there exists a unique pair of solutions to (3.5), in the set of smooth functions with sufficiently small energy $\mathcal{F}[U] = O(\varepsilon)$, which are identical up to a reflection $u \to -u$. Hence for initial data with small enough energy, we expect the solution of the initial boundary value problem to converge to one of these stationary states, namely the one closer to the initial data. We can check this by superimposing the solution for (3.5) onto the long-time profile for the initial boundary value problem. In addition, the stationary solution $U(r)$ exceeds 1 by an $O(\varepsilon)$ amount. This fact, which is a manifestation of the Gibbs–Thomson

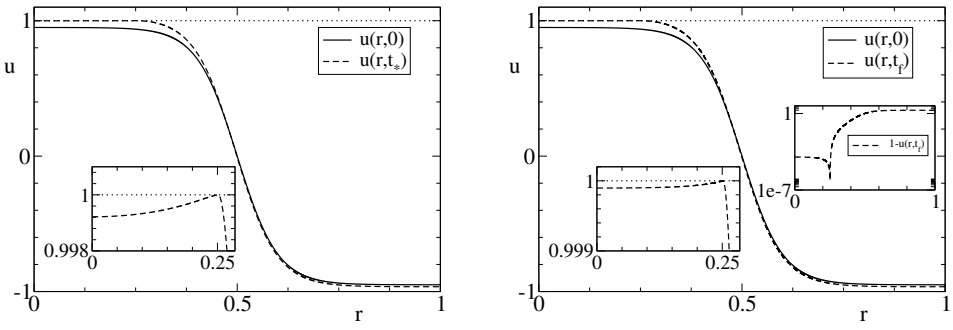

FIG. 2. *Left: Solution u of* (2.1) *with degenerate mobility $n = 1$, for the initial time ($t = 0$) and after the touchdown, as illustrated by the zoom in the inset. See* (3.7). *Right: Solution of* (2.1) *with mobility $n = 4$, for the initial time and for $t = t_{final} = 10^{15}$, when we stopped the simulation (though it could still have been continued). The maximum of u is very close to the value $u = 1$ (see bottom left inset), but, as a semilog plot of $1 - u$ in the top right inset reveals, has touched there.*

effect [31, 53], is often missed, but it is an important feature of the evolution. It basically precludes the possibility that $|u| < 1 - \delta$ pointwise for some positive δ. If that were the case, the small-energy stationary profile to which the solution converges would be strictly bounded by $|u| < 1$, contradicting the result in [60]. This is a strong indication that $|u| \to 1$ at some point(s) r_* and at either a time $t_* < \infty$ or at the limit $t \to \infty$. We refer to these two cases as finite-time and infinite-time touchdown, respectively. For constant mobility, the former of the two occurs.

Degenerate mobilities with $n = 1$. The numerical solution behaves similarly to the constant mobility case in that $\max_r u$ reaches 1 in finite time, at $t = t_* = 3.44$ for a grid spacing of $\Delta r = 10^{-4}$; see Figure 2, left, and the inset. However, we noticed that t_* increases significantly upon decreasing Δr, suggesting the possibility that this finite-time touchdown is a numerical artifact and that for $\Delta r \to 0$, the value $t_* \to \infty$ and hence that the numerical solution converges to an infinite-time touchdown solution.

Finite-time touchdowns—or in fact crossings—of $|u| = 1$ have been reported in the literature. For example, for the fully two-dimensional simulations in [33], where the authors use an absolute value mobility (2.3), the solution u crosses the bound $|u| = 1$ on the convex side of interfaces between different phases and converges to a quasi-stationary profile with a larger value than the one as predicted by the Gibbs–Thomson effect. Other analytical results [38] prove existence of solutions $u \leq 1$, which allow for touchdowns but not for crossings into $|u| > 1$. The occurrence of qualitative different behaviors for one initial value problem is consistent with the nonuniqueness of solutions that is known to occur for initial value problems of high-order degenerate parabolic PDEs in the Cahn–Hilliard and thin film context; see, for example, [32, 30, 49, 10, 34].

Moreover, where the solution achieves a value for which the mobility vanishes, it typically loses regularity. This can be illustrated by a formal argument made for a Hele-Shaw model in [27] (see also a rigorous version in [28] and a similar argument for a more general thin film problem in [14]), applied here to $v := 1 - u$. Letting $n = 1$, at the minimum $r = \bar{r}(t)$ of v at time t, which we denote $\bar{v}(t) := v(\bar{r}(t), t)$, we have that

$$\frac{1}{2}\frac{\mathrm{d}}{\mathrm{d}t}\ln\left(\frac{2-\bar{v}}{\bar{v}}\right) = \frac{1}{r}\partial_r\left(r\partial_r\mu\right)\Big|_{r=\bar{r}(t)}. \tag{3.9}$$

When $\bar{v}(t) \to 0$, the left-hand side blows up and the second derivative of μ, and hence the fourth derivative of v (or u), must do so too. The argument can also be extended to $n > 1$ by computing instead $\frac{\mathrm{d}}{\mathrm{d}t}\left(\bar{v}^{1-n}\right)$. As a consequence, rigorous treatments of (1.1a), (2.1e), and (2.2) or (2.3) introduce weak formulations and then typically prove existence of such solutions via regularization of the degeneracy, with different outcomes depending on the details of the weak formulation and the regularization method. In [38], for example, the authors prove existence of solutions for $n \geq 1$ that satisfy $|u| \leq 1$, using a regularized version of (2.2), while in [32], Dai and Du introduce a weak solution concept and a regularization of the mobility (2.3) that allows for solutions where $|u|$ can exceed 1. This is consistent with the solutions they present in their numerical study [33].

At this stage one may ask if the vanishing of the mobility along the solution can be avoided, so that, for example, the existence of solutions with $|u| \leq 1$ by Elliott and Garcke [38] can be strengthened to show the existence of a solution u for which $|u|$ stays strictly below 1 even in the limit as $t \to \infty$. However, in the preceding section on the constant mobility case, we gave an argument that rules out convergence to a stationary solution with modulus less than $1-\delta$ for some $\delta > 0$, which also carries over to the degenerate case $n > 0$. This implies that the solution (provided it converges to a stationary solution) either achieves $\max_r |u| = 1$ in finite time or converges as $\max_r |u| \to 1$ in infinite time.

Degenerate mobilities with $n = 4$. As before, a maximum forms in the numerical solution that approaches $u = 1$ at some point $r = \bar{r}(t)$, but $1-u$ remains positive over many decades of t. In Figure 2, right, u still has not touched $u = 1$ at $t = 10^{15}$. This suggests that the singularity is only approached in infinite time. Moreover, the PDE remains strictly parabolic and hence we expect it to have a unique classical solution, that is, the same evolution should emerge for any other convergent numerical scheme.

In the following, we investigate the behavior shown by this third example in more detail numerically and via asymptotic analysis for the long-time limit $t \to \infty$, to conclude that the numerical solutions of (2.1), (2.1f), (3.1) converge to a leading order asymptotic approximation that touches down in infinite time (and remains bounded away from $|u| = 1$ for any finite value of t).

3.1. Self-similar regions. We consider numerical results for three different values of $n = 3, 4, 5$, with the aim of investigating the structure of the solution at large times. To characterize the evolution as $t \to \infty$, we let $v = 1 - u$ and zoom in to the regions of $r \in (0, 1)$ where $|v|$ is small. We first observe that the region of v closer to $r = 0$, which we refer to as the central region, evolves differently from the touchdown region near $r = \bar{r}(t)$. There, the solution has a pronounced minimum $v(\bar{r}(t), t)$, and the function decreases more rapidly than for $v(0, t)$. In fact, the log-log plot in Figure 3 suggests that $v(0, t)$ and $v(\bar{r}(t), t)$ display a power law behavior for large t. Furthermore, both regions keep their qualitative shape, prompting us to seek self-similar solutions with power law scaling factors.

In the central region, we specifically make the ansatz

$$v(r, t) \sim t^{\alpha} \psi(r) \tag{3.10}$$

with some $\alpha < 0$. The independent variable is not scaled as the region it spans extends from $r = 0$ to near $\bar{r}(t)$, which is an $O(1)$ interval. The scaling (3.10) can be tested by plotting $v(r, t)/v(0, t)$ in Figure 4, left, where we observe that all curves collapse near $r = 0$. Moreover, the location of the minimum of v, i.e., $r = \bar{r}(t)$, appears to converge to a limit, which we denote by r_* for future reference. Here this limit is approximately $r_* = 0.25$.

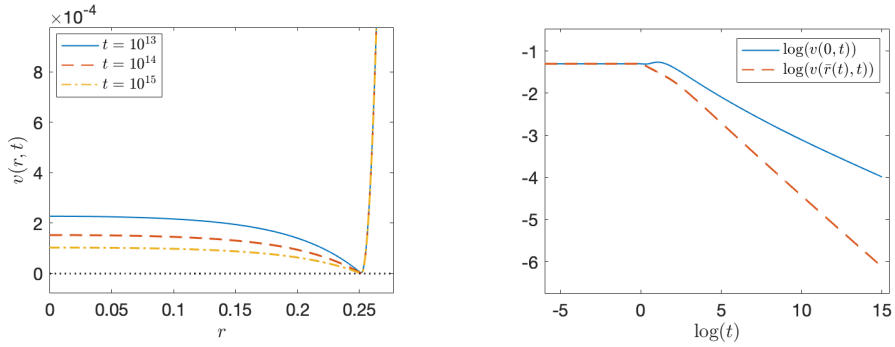

FIG. 3. *Left: The profile $v = 1 - u$ for the solution of* (2.1) *with mobility $n = 4$, for different times. The dotted line represents the* 0 *value line. Right: Evolution of $v(0,t)$ and $v(\bar{r}(t),t)$ in a log-log plot.*

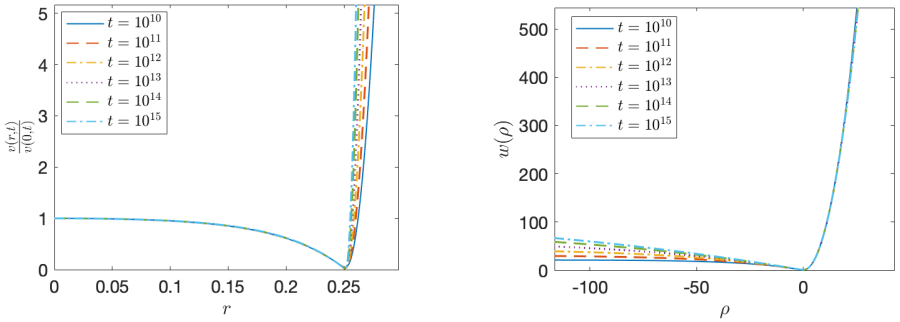

FIG. 4. *Left: Central region rescaled according to r versus $v(r,t)/v(0,t)$ for different times Right: Rescaled touchdown region, w versus ρ, for the same times as in* (a). *The definition of w and ρ are given in the main text.*

In the touchdown region, we introduce a scaling for both variables, so that

$$v(r,t) \sim t^{\beta}\varphi(\eta), \qquad \eta := \frac{r - r_*}{t^{\gamma}}, \tag{3.11}$$

for some β, $\gamma < 0$. We test the self-similar scaling by scaling

$$w := \frac{v(r,t)}{\min\limits_{r\in[0,1]} v(t)}$$

so that the minimum value of the new function is now 1 for all t. If $\bar{r}(t)$ is, as before, the point where this minimum is located, and if $r = \bar{r}(t) + \Delta r(t)$, with $\Delta r(t) > 0$, is the point where $w(r,t) = 3$, then we define the rescaled independent variable as

$$\rho = \frac{(r - \bar{r}(t))}{\Delta r(t)}.$$

Plotting w versus ρ, we clearly see in Figure 4, right, that around $\rho = 0$, the curves collapse nicely over at least three orders of magnitude $t = 10^{10}, \ldots, 10^{15}$.

Similarity exponent for the central region. Next, we determine the approximate numerical values for α, β, and γ from the numerical data in the central and touchdown regions. We first look at log-log plots for $v(0,t)$ for three different values of n. The

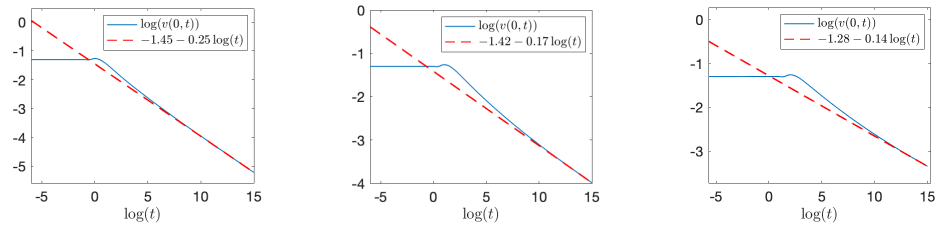

FIG. 5. *Linear fitting of* $\log(v(0,t))$ *versus* $\log(t)$ *for* $\varepsilon = 0.1$. *Left:* $n = 3$*; middle:* $n = 4$*; right:* $n = 5$.

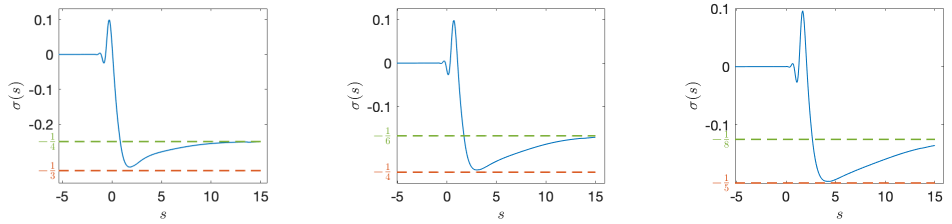

FIG. 6. *Numerical approximation* σ *for the power law exponent versus* s *up to the final time* $t_{final} = 10^{15}$ *where we ended the simulation, and* $\varepsilon = 0.1$. *Left: for* $n = 3$*; middle:* $n = 4$*; right:* $n = 5$. *Definitions of* σ *and* s *are given in the main text; see* (3.12).

result is shown in Figure 5 for $n = 3, 4, 5$. We see that for long times $\log v(0,t)$ is linear in $\log t$, though it appears that two different slopes emerge at different times. To analyze this further, in Figure 6 we also plot

$$\sigma(s) := \frac{\mathrm{d}\log v(0,t)}{\mathrm{d}s}, \qquad s := \log t, \tag{3.12}$$

which gives the effective exponent of a power-law behavior (for a pure power law, $\sigma(s)$ would be constant and exactly equal to the exponent). It is clear in Figure 6 that σ takes a dip, with the minimum at $-1/3$, $-1/4$, $-1/5$ for $n = 3$, 4, and 5, respectively, suggesting that for general n, $\sigma = -1/n$ at its minimum value. However, this is a transient in the sense that after the minimum, σ increases again and then tends to $-1/4$, $-1/6$, $-1/8$ for the three values of n. This indicates that for very long times, in general, we have

$$\alpha = -\frac{1}{2(n-1)}. \tag{3.13}$$

Similarity exponents for the touchdown region. In the touchdown region, the log-log plot for $v(\bar{r}(t), t)$ in Figure 7 reveals that, for long times, the evolution of this value indeed approaches a power-law behavior. As in the central region, approximations for the similarity exponent β can be extracted from

$$\sigma_*(s) := \frac{\mathrm{d}\log v(\bar{r}(t), t)}{\mathrm{d}s}.$$

Note that even though the touchdown region should be centered at $r_* = \lim_{t\to\infty} \bar{r}(t)$, because we do not know its value a priori, we must use instead $\bar{r}(t)$. The result is

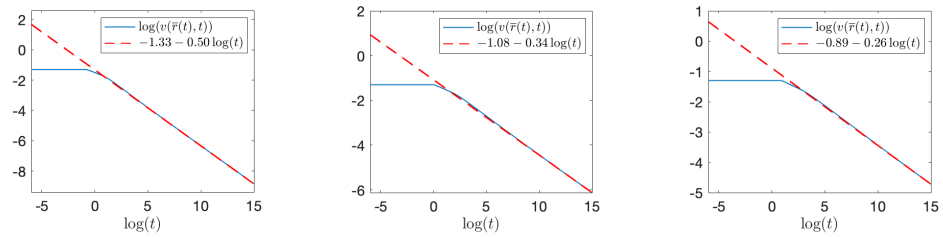

FIG. 7. *Linear fitting for* $\log(v(\bar{r}(t),t))$ *versus* $\log(t)$ *for* $\varepsilon = 0.1$. *Left:* $n = 3$*; middle:* $n = 4$*; right:* $n = 5$.

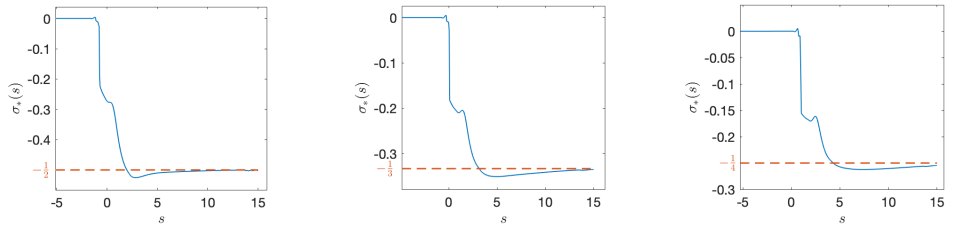

FIG. 8. *Numerical approximation* σ_* *for the power law exponent up to the final time* $t_{final} = 10^{15}$ *where we stopped the simulation, and* $\varepsilon = 0.1$*, for (left)* $n = 3$*, (middle)* $n = 4$*, and (right)* $n = 5$. *Definitions of* σ_* *and* s *are in the main text.*

shown in Figure 8, where σ_* approaches $-1/2$, $-1/3$, and $-1/4$ for the three values $n = 3, 4, 5$, respectively. This is consistent with

$$\beta = -\frac{1}{n-1}. \tag{3.14}$$

On the other hand, we obtained that $\partial_{rr} v(\bar{r}(t), t)$ tends to a constant as $t \to \infty$. Since $\partial_{rr} v(\bar{r}(t), t) \propto t^{\beta - 2\gamma}$, this means $\beta = 2\gamma$, and thus

$$\gamma = -\frac{1}{2(n-1)}. \tag{3.15}$$

Varying ε. We conclude our numerical exploration by studying the effect of varying ε for fixed $n = 4$. Results are shown in Figure 9 for $\sigma(s)$ and $\sigma_*(s)$ for a range of $\varepsilon \leq 1$. All curves show the two self-similar scalings that we already reported on earlier. In the left figure, σ approaches a minimum $-1/n$ first and eventually the value for α in (3.13). The time it takes to move from the minimum close to the final asymptotic value increases as ε decreases. A similar observation is made in the right figure for σ_* and its approach to β as in (3.14), except that here, the minimum itself shifts as ε is decreased.

4. Long-time asymptotic analysis for $n > 2$. In this section we carry out a long-time asymptotic analysis of the solution to (2.1), via singular perturbation theory. For the purpose of carrying out the long-time expansion, it is helpful to separate magnitude from variable by introducing the scaling

$$t = \tau/\delta. \tag{4.1}$$

We then seek expansions in terms of $0 < \delta \ll 1$ as the small parameter, with fixed τ. We note that while ε is also small, we treat it as a fixed parameter.

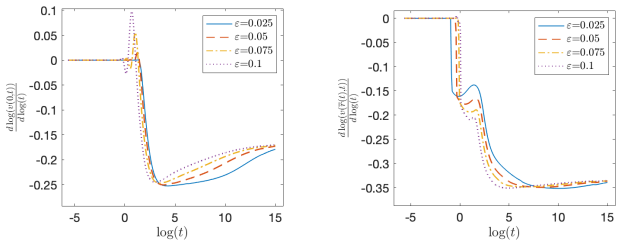

FIG. 9. *Impact of ε on the evolution into the final self-similar behavior in the central and touchdown regions. In both cases, $n = 4$. Left: results for σ the central region; right: results for σ_* in the touchdown region.*

We first formulate the leading order problem in each of the three regions—central, touchdown, and annular—and solve and match them. Then we construct the composite solution and compare it with the numerical results.

For the central and touchdown regions, it is convenient to formulate the problem in terms of the function $v = 1 - u$. Since we are interested in solutions that are bounded $|u(r,t)| \leq 1$ for all $r \in (-0,1)$, $t \in (0,\infty)$, we look for nonnegative v. Substituting v into (2.1a), (2.1b), (2.1c), (2.1e), (2.1f) and rescaling time according to (4.1) we obtain

$$\delta \partial_\tau v = -\frac{1}{r}\partial_r \left(rM(v)\partial_r \mu\right), \tag{4.2a}$$

$$\mu = \varepsilon^2 \left(\partial_{rr} v + \frac{1}{r}\partial_r v\right) + 2(-v^3 + 3v^2 - 2v) \tag{4.2b}$$

with boundary conditions

$$\partial_r v(1,t) = 0, \tag{4.2c}$$

$$M(v(1,t))\partial_r \mu(1,t) = 0, \tag{4.2d}$$

$$\partial_r v(0,t) = 0, \tag{4.2e}$$

$$\partial_r \mu(0,t) = 0, \tag{4.2f}$$

where $M(v) = v^n(2-v)_+^n$, for $n > 2$. For later uses, we record that the radial flux is given by

$$j = -M(v)\partial_r \mu. \tag{4.2g}$$

4.1. Central region. We start from (4.2) and assume, using the insight gained from the numerical results, that v can be expanded as

$$v_{\text{central}}(r,\tau) = \delta^{-\alpha}\tau^\alpha \psi_0(r) + o(\delta^{-\alpha}), \tag{4.3}$$

where $\alpha \in \mathbb{R}$ and ψ_0 is a nonnegative function. Since the solution must be bounded as $\delta \to 0$, we restrict our attention to $\alpha < 0$.

We substitute (4.3) into (4.2a), (4.2b), combine the equations into a single one by eliminating μ, and drop all terms that we already know are of lower order to get

$$\alpha\delta^{-\alpha+1}\tau^{\alpha-1}\psi_0 = -\delta^{-(n+1)\alpha}\tau^{(n+1)\alpha}\frac{2^n}{r}\partial_r\left[r\psi_0^n\partial_r\left(\varepsilon^2\frac{1}{r}\partial_r\left(r\partial_r\psi_0\right) - 4\psi_0\right)\right]. \tag{4.4}$$

Balancing both sides would require $\alpha = -1/n$, but this is not consistent with the numerical results, for which α is clearly larger. In that case, the right-hand side of the equation dominates the left-hand side, so that we obtain, after integrating twice with respect to r and using the Neumann boundary condition at the origin (4.2f), the leading order problem

$$\varepsilon^2 \left(\partial_{rr}\psi_0(r) + \frac{1}{r}\partial_r \psi_0(r) \right) - 4\psi_0(r) = c_1, \tag{4.5a}$$

$$\partial_r \psi_0(0) = 0, \tag{4.5b}$$

where c_1 is an unknown constant that comes from the second integration. The general solution of (4.5a)–(4.5b) can be directly computed as

$$\psi_0(r) = -\frac{c_1}{4} + c_2 I_0\left(\frac{2}{\varepsilon} r\right),$$

where I_0 is the *modified* Bessel function of the first kind and c_2 is another unknown constant of integration.

This solution will be matched to the one in the touchdown region, which plays the role of an inner expansion where the dependent variable is small (in terms of $\delta \ll 1$) compared to the expansion in the central region. Thus, ψ_0 must vanish at $r = r_*$, that is,

$$\psi_0(r_*) = 0,$$

which we use to eliminate c_1, giving

$$\psi_0(r) = c_2 \left(I_0\left(\frac{2}{\varepsilon} r\right) - I_0\left(\frac{2}{\varepsilon} r_*\right) \right). \tag{4.6}$$

This expression is, of course, only valid for $0 \le r \le r_*$; we extend it by $\psi_0 = 0$ for $r_* < r \le 1$ where this is needed (for example, in the evaluation of the composite expansion). The remaining constant, c_2, represents a normalization of v that we keep as a parameter and that we fix when we numerically solve the problem in the touchdown region. For later, we record that the Taylor expansion of ψ_0 near r_* is

$$\psi_0(r) = a_1(r - r_*) + O((r - r_*)^2), \qquad a_1 = \frac{2c_2}{\varepsilon} I_0'\left(\frac{2}{\varepsilon} r_*\right). \tag{4.7}$$

4.2. Touchdown region. In this region, we introduce the independent variable

$$\eta = \frac{r - r_*}{\delta^{-\gamma}\tau^{\gamma}}, \tag{4.8}$$

with $\gamma < 0$, and expand

$$v_{\text{touchdown}} = \delta^{-\beta}\tau^{\beta}\varphi_0(\eta) + o(\delta^{-\beta}), \tag{4.9}$$

where $\beta < 0$, as suggested by our previous numerical results, and φ_0 is a nonnegative function. Dropping higher order terms and eliminating μ gives

$$\delta^{1-\beta}(-\gamma\eta\tau^{-1}\partial_\eta\varphi_0) = -\varepsilon^2 \frac{\delta^{4\gamma-(n+1)\beta}\tau^{-4\gamma}2^n}{\eta\left(\frac{\tau}{\delta}\right)^{\gamma} + r_*} \partial_\eta \left(\left(\eta\left(\frac{\tau}{\delta}\right)^{\gamma} + r_* \right) \varphi_0^n \partial_{\eta\eta\eta}\varphi_0 \right).$$

There are three possibilities here: either the left-hand side goes to zero faster than the right-hand side, and hence $\beta > \frac{4\gamma-1}{n}$, the other way around, thus $\beta < \frac{4\gamma-1}{n}$, or they balance each other with $\beta = \frac{4\gamma-1}{n}$. From our previous numerical results, we can infer that the first case is the relevant one. Integrating the resulting leading order long-time equation once, we arrive at the ODE

$$\varphi_0^n(\eta)\partial_{\eta\eta\eta}\varphi_0(\eta) = J, \tag{4.10}$$

where the unknown flux J appears as an integration constant. This third order problem has to be matched to the central (as $\eta \to -\infty$) and annular (as $\eta \to \infty$) regions, which both act as larger, i.e., outer, layers. To match to a leading order $O(1)$ contribution in the annular region, the leading order term of $\varphi_0(\eta)$ must be $\sim \eta^{\beta/\gamma}$ for $\eta \to \infty$, so that upon scaling back into annular variables, the δ-factors cancel. From the numerical results, we have already observed that β/γ is closer to 2 than to 1, hence φ_0 grows faster than linear, and this selects the behavior of the annular solution to be quadratic near r_*.

4.3. Annular region. In the numerical simulations we saw that the solution evolves much slower to the right of $\overline{r}(t)$, at least compared with the central and touchdown regions. This leads us to believe that a good first approximation in the interval $(r_*, 1)$ is given by the stationary problem. For the annular region, we expect a stationary solution to leading order, as the only time dependence comes from the slow drainage of material from the central region. This is supported by the numerical evidence, and therefore we let for the leading order annular solution

$$v_{\text{annular}}(r,\tau) = 1 - U_*(r). \tag{4.11}$$

Substituting into (4.2a)–(4.2f) and integrating twice, we obtain

$$-\frac{\varepsilon^2}{r}\frac{d}{dr}\left(r\frac{dU_*}{dr}\right) - 2U_*(1-U_*^2) = \mu_0, \tag{4.12a}$$

$$\frac{dU_*}{dr}(1) = 0, \tag{4.12b}$$

for $r \in (r_*, 1)$, where μ_0 is an unknown integration constant. The solutions can be locally expanded in a Taylor series, which does not have a constant or linear contribution to be matchable to the touchdown region, which grows superlinearly as observed in the previous section. Thus

$$U_*(r_*) = 1, \quad \frac{dU_*}{dr}(r_*) = 0. \tag{4.12c}$$

For $r \in [0, r_*]$ we set the solution to $U_* \equiv 1$. Note that this is exactly the problem treated by Lee, Münch, and Süli [53]. From (4.12a) and (4.12c), we obtain the leading term in the Taylor series expansion for v_{annular},

$$v_{\text{annular}} = b_2(r-r_*)^2 + O((r-r_*)^3), \qquad b_2 = \frac{\mu_0}{2\varepsilon^2}. \tag{4.13}$$

4.4. Matching.

Central and touchdown region. We first match the central and touchdown solutions. First, we expand the inner expansion of v_{central} as $r \to r_*$ and rewrite the result in terms of η, giving

$$v_{\text{central}} = \delta^{-\alpha}\tau^{\alpha}a_1(r - r_*) + \text{h.o.t.} = \delta^{-\gamma-\alpha}\tau^{\alpha+\gamma}a_1\eta + \text{h.o.t.}, \tag{4.14}$$

where we recall that a_1 is given in terms of r_* via the modified Bessel function; see (4.7). This has to be matched with

$$v_{\text{touchdown}} = \delta^{-\beta}\tau^{\beta}A_-\eta + \text{h.o.t.}, \tag{4.15}$$

and therefore

$$\beta = \alpha + \gamma, \qquad A_- = a_1. \tag{4.16}$$

Annular and touchdown region. On the other side of r_*, we know that v_{annular} has a Taylor expansion as $r \to r_*$ that starts quadratically, hence

$$v_{\text{annular}} = b_2\delta^{-2\gamma}\tau^{2\gamma}\eta^2 + \text{h.o.t.}, \tag{4.17}$$

where again b_2 is known from (4.12) in terms of r_*. Thus, the expansion of the solution in the touchdown region at $\eta \to \infty$ must also be quadratic,

$$v_{\text{touchdown}} = \delta^{-\beta}\tau^{\beta}A_+\eta^2 + \text{h.o.t.}, \tag{4.18}$$

and completing the matching requires

$$\beta = 2\gamma, \qquad A_+ = b_2. \tag{4.19}$$

Matching of the flux between central and touchdown region. So far, we have only got two relations for α, β, and γ; we need one more to completely fix the similarity exponents. One can obtain a partial mass conservation condition in the interval $(0, r_*)$ by multiplying (4.2a) by r, then integrating in $r \in (0, r_*)$ and using the boundary condition at $r = 0$ (4.2f). This gives

$$\int_0^{r_*} \partial_t v(r,t) r dr = -r_* M(v(r_*,t))\partial_r \mu(r_*,t).$$

This means that the rate of change in mass in the interval $(0, r_*)$ is equivalent to the flux at r_*. We rescale the right-hand side into touchdown variables and use the leading order asymptotic solutions (4.3) and (4.9) to obtain

$$-\alpha\delta^{-\alpha+1}\tau^{\alpha-1}\frac{c_2 r^{*^2}}{2} I_2\left(\frac{2r_*}{\varepsilon}\right) = -r_*\delta^{-\beta(n+1)+3\gamma}\tau^{\beta(n+1)-3\gamma}2^n\varepsilon^2 J,$$

and, therefore, matching requires

$$\alpha - 1 = \beta(n+1) - 3\gamma, \tag{4.20}$$

$$J = \alpha\frac{c_2 r_*}{2^{n+1}\varepsilon^2} I_2\left(\frac{2r_*}{\varepsilon}\right). \tag{4.21}$$

We note that this could also be obtained from matching at higher order in the expansions instead of using the mass conservation derived from the equation. The solution to (4.16), (4.19), (4.20) is

$$\alpha = \gamma = -\frac{1}{2(n-1)}, \quad \beta = -\frac{1}{n-1}. \tag{4.22}$$

These are exactly the values that we observed in the numerical results in section.

4.5. Solution in the touchdown region. We analyze the touchdown region in more detail to ensure that a solution can be obtained, at least numerically, that satisfies all the matching conditions. In particular, we carry out an overall degree of freedom count and briefly explain how we solve for ϕ_0.

The expansions of solutions ϕ_0 of (4.10) for large negative and positive arguments can be obtained from the literature (see, e.g., the systematic study of such expansions for thin film type equations in [18]), but to be self-contained, we give a derivation in the appendix for the case of linear leading order as $\eta \to -\infty$ and quadratic leading order for $\eta \to \infty$. In summary, within the $n > 2$ case we have the following subcases:

$$\varphi_0(\eta) = \begin{cases} A_-\eta + \frac{JA_-^{-n}(-\eta)^{3-n}}{(n-1)(n-2)(n-3)} + B_- + O(1) & \text{if } 2 < n < 3, \\ A_-\eta + \frac{J}{2A_-^3}\ln(-\eta) + B_- + O(1) & \text{if } n = 3, \\ A_-\eta + B_- + O(1) & \text{if } n > 3, \end{cases} \tag{4.23a}$$

as $\eta \to -\infty$, and

$$\varphi_0(\eta) = A_+\eta^2 + B_+\eta + C_+ + O(1) \quad \text{for } n > 3/2 \quad \text{as } \eta \to \infty, \tag{4.23b}$$

where $A_\pm$, $B_\pm$, C_+, J are unknown constants. The limitations on n arise from the requirement that the correction terms must be asymptotically small compared to the leading order term. In particular, the leading order linear expansion for large negative arguments is only valid for $n > 2$ and sets the lower bound for n that we consider in this study.

The degree of freedom count is as follows: We have six unknown constants, $A_\pm$, $B_\pm$, C_+, and J. Two of them (A_+ and A_-) have been fixed by matching to the appropriate outer problems, though this introduces additional unknowns, which we will return to later. The third order differential equation takes care of another three degrees of freedom, so that only one is left. This degree of freedom is the result of the ODE (4.10) being autonomous and represents an arbitrary shift of the solution. This shift is fixed by the requirement that η is defined in (3.1) through the position r_* where v touches down (for $t \to \infty$). Hence φ_0 must have its minimum at $\eta = 0$.

Returning first to A_-, we see that matching specifies this constant in terms of c_2 and r_* (see (4.7) and (4.16)), but we can use (4.21) to eliminate c_2. For A_+, (4.19) and (4.13) introduce a dependence on μ_0. However, both r_* and μ_0 are completely determined by solving the leading order problem in the annular region (4.13), (4.12) if this is supplemented by an overall mass constraint. Hence after matching all layers, the solutions in all regions are completely determined.

The solution strategy for the touchdown region is as follows. We consider (4.10) first with the condition (4.13). Since B_- represents a translation in η we do not need to enforce its value and only impose the leading order behavior $A_-\eta$. By rescaling

$$\varphi_0(\eta) = c\phi_0(y), \quad \eta = dy,$$

with

$$c := \left(\frac{J}{(-A_-)^3}\right)^{\frac{1}{n-2}} > 0, \quad d := \left(\frac{J}{(-A_-)^{n+1}}\right)^{\frac{1}{n-2}} > 0,$$

we see that ϕ_0 satisfies the parameter-free problem

$$\phi_0^n(y)\partial_{yyy}\phi_0(y) = 1, \quad y \in (-\infty, \infty), \tag{4.24a}$$

(4.24b) $$\phi_0(y) = -y \text{ as } y \to -\infty,$$

and read off $\kappa = \partial_{yy}\phi_0(y_0)$ from the numerical solution. Scaling back and using (4.19), (4.13) gives

$$\frac{\mu_0}{\varepsilon^2} = 2A_+ = \kappa \frac{c}{d^2}.$$

This is essentially an equation between J, A_-, and μ_0, the latter being fixed by the annular region. Replacing $A_- = a_1$ by the second equation in (4.7) and using (4.21), we obtain the expression for c_2

$$c_2 = -\left| \frac{\mu_0^{n-2}\varepsilon I_2\left(\frac{2r_*}{\varepsilon}\right)}{2^{3n+1}(n-1)\kappa^{n-2} I_1\left(\frac{2r_*}{\varepsilon}\right)^{2n-1}} \right|^{\frac{1}{2(n-1)}},$$

which now fixes c_2 once μ_0 and r_* have been obtained by solving the annular problem. Numerically, (4.24) is solved on a large truncated domain and then extended, where necessary, to an infinite domain by using the expansions (4.23a), (4.23b).

4.6. Solution in the annular region. The solution in the annular region also needs to be obtained numerically. As noted in [53] we need an extra condition to solve for the unknown μ_0, which may be obtained by either fixing the position of the interface or adding a mass constraint. We choose the latter and impose

(4.25) $$\int_{r_*}^{1} U_*(s) s \, ds = m_0 - \frac{r_*^2}{2},$$

with m_0 is the initial mass, as defined in (3.8). The problem (4.12), (4.25) is then solved by picking r_*, solving all conditions except for (4.25) using the MATLAB solver bvp4c, and then iterating over r_* until the mass constraint is satisfied, too. Practical details, such as the conversion into a boundary value problem for a system of first order ODEs, are discussed in an appendix. For the problem here, we obtain a solution with the required mass for $r_* = 0.2516$.

4.7. Composite approximation. We now construct the composite approximation from the asymptotic solutions found in the previous sections. We add each of the approximations—central, touchdown, and annular—in the same variables and subtract common terms; in other words,

(4.26) $$\begin{aligned} v_{\text{comp}}(r,t) =& v_{\text{central}}(r,t) + v_{\text{touchdown}}(r,t) + v_{\text{annular}}(r,t) \\ & - A_- t^{\alpha}(r-r_*)_- - A_+(r-r_*)_+^2. \end{aligned}$$

The subscript "$-$" ("$+$") means that we take the value of the brackets where it is negative (positive) and zero elsewhere.

In Figure 10 we present the leading order of the composite expansion at two times, $t_1 = 10^{13}$ and $t_2 = 10^{15}$, and compare them with the numerical PDE solution for $r \in [0,1]$ at both times. We use a semilog plot on the right so that all relevant parts of the solution, which differ by several orders of magnitude, can be shown in a single plot. Note that we only use the PDE solution for comparison and the only external data that is fed into the computation of composite expansion is the mass of the initial condition m_0. The composite solution closely follows the numerical solution of the full problem for v in the whole interval $[0,1]$. The agreement is excellent, as shown in Figure 10, at times $t = t_1$ and t_2. In fact, the overall agreement becomes better at the later time, $t = t_2$, as the absolute error

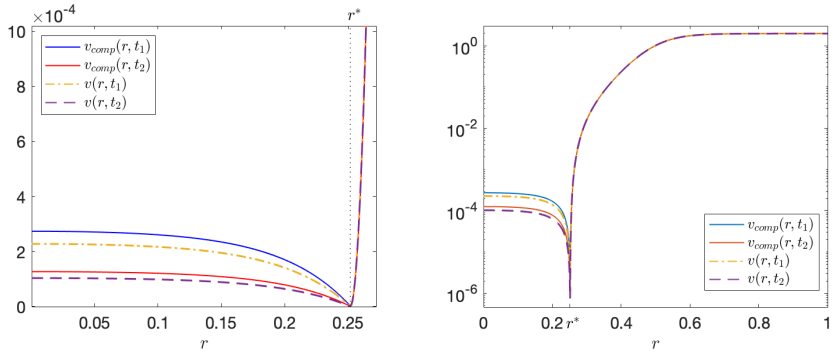

FIG. 10. *Left: Plot of v_{comp} v/s r compared to numerical PDE solution v, for $t_1 = 10^{13}$, $t_2 = 10^{15}$, $\Delta r = 10^{-6}$, $n = 4$, $\varepsilon = 0.1$, and $r_* = 0.2516$. Right: Comparison of v_{comp} with the PDE solution, on a scale that shows the complete solution. Parameter values and times carry over from the left.*

$$\text{error}(t) = \max_{r\in[0,1]} |v(r,t) - v_{\text{comp}}(r,t)| \tag{4.27}$$

decreases between t_1 and t_2.

5. Discussion and outlook. While the spontaneous appearance of touchdowns, that is, the emergence of points $\{M(u) = 0\}$ for the degenerate Cahn–Hilliard equation, is a well-known phenomenon in the development of numerical algorithms for these types of PDEs, so far, they have been addressed by ad hoc measures such as adding a small positive constant to the mobility; see, for example, [72]. In this study, we systematically investigate how such points of vanishing mobility arise. Important results of this work are that small energy solutions to the degenerate Cahn–Hilliard problem (2.1) touch down, in either finite or infinite time, and that for $n > 2$ and practically relevant tanh-like initial data, the solution converges to a long-time profile that touches down in infinite time, suggesting this is the generic behavior for large enough values of n. Our asymptotic analysis also revealed that for $n \leq 2$, the asymptotic structure of the solution changes so that these values of $n \leq 2$ require a separate investigation, which will appear in an upcoming paper. There it is shown that asymptotic approximations for infinite-time touchdown solutions can be found also for $1/2 < n \leq 2$. Based on the experience with thin film problems with pressure boundary conditions [14], however, these solutions could become increasingly fragile closer to $n = 1/2$, and finite time solutions are more likely to emerge.

Future work could investigate fully two-dimensional situations and nonconvex interfaces between the phases, and the impact of touchdown regions on the sharp interface evolution. For finite-time touchdown, once the solution has reached $|u| = 1$, further questions arise about how to continue the solution, noting that already more than one weak solution concept has been considered in the literature [38, 32]. Also, thin film theory could provide insight into how to construct numerical schemes that maintain $|u| < 1$, e.g., [79, 44]. Another avenue of research could be to introduce a further parameter by taking $f(u) = (1 - u^2)^m$ with $m \geq 2$ and exploring the singularity formation depending on the degree of degeneracy of both n and m. This could lead to a parameter plane for (m, n) with an additional interesting structure. Similar studies have been done for solutions of thin film equations [16, 40, 47].

More generally, our study underscores the close connection of degenerate Cahn–Hilliard equations with thin film models, and the still untapped potential for using

not only the rigorous proofs but also the asymptotic results from thin film theory to understand singularity formation in degenerate Cahn–Hilliard models. Inside a spherically symmetric phase domain (more generally, convex domain) in the late stages of phase separation, the degenerate Cahn–Hilliard model is closely related to the thin film equation with pressure boundary conditions [14] and hence the points with vanishing mobility can be analyzed in a similar way. This opens up a rich source of analytical tools, both asymptotic and rigorous, that we can apply to degenerate Cahn–Hilliard problems [27, 28, 10, 12].

Appendix A. Expansion of ϕ_0 for large arguments.

Expansion at $\eta \to -\infty$. We let $x = -\eta$ and look for an expansion of $\phi(x) := \varphi_0(\eta)$ such that

$$\phi^n \phi''' = -J, \tag{A.1}$$

as $x \to \infty$, where $'$ denotes derivatives with respect to x.

Starting with the expansion $\phi(x) = Ax + \xi(x)$ with $\xi \ll x$ as $x \to \infty$ gives, upon substituting this ansatz into (A.1) and balancing, the following corrections:

$$\xi(x) = \frac{-J}{A^n(n-1)(n-2)(n-3)} x^{3-n} + B, \tag{A.2}$$

where B is a constant, provided $n \neq 3$. We note that the first term dominates the second if $n < 3$, and vice versa if $n > 3$. Consistency between the leading order and correction requires that $3 - n < 1$, i.e., $n > 2$, because only then we have that $\xi \ll x$. Moreover, if $n = 3$, the confluence of x^{3-n} and the contribution from x^p with $p = 0$ produces a logarithmic term, that is,

$$\xi(x) = \frac{-J}{2A^3} \ln(x) + B. \tag{A.3}$$

Returning to the original variables then gives (4.23a).

Expansion at $\eta \to \infty$. For $\eta \to \infty$ we are looking for an expansion of solutions of (4.10) starting with a quadratic term, where $'$ denotes derivatives with respect to η. We make the ansatz

$$\varphi_0(\eta) = A\eta^2 + \xi(\eta)$$

with $\xi \ll \eta^2$ and A a constant. Introducing this into the differential equation, we obtain

$$\xi(\eta) = D\eta + \frac{-J}{A^n(2n-1)(2n-2)(2n-3)} \eta^{3-2n} + E, \tag{A.4}$$

where D and E are unknown constants. For $n \leq 1/2$, the second term grows faster than quadratic and therefore the expansion of ϕ_0 is not consistent. Hence we require $n > 1/2$. Note that the order of the terms in (A.4) changes as the values $n = 3/2$ and $n = 1$. If $n > 3/2$, the term proportional to J decays for large η and therefore in this case the first three terms in the $\eta \to \infty$ expansion of ϕ_0 are as claimed in (4.23b).

Appendix B. Details of the numerical approach in the annular region. We define

$$S(r) := \int_{r_*}^{r} U_*(s) s \, ds.$$

Then the system (4.12) with (4.25) can be written as

$$S' = U_* r, \tag{B.1a}$$

$$U_*' = W, \tag{B.1b}$$

$$W' = \frac{2}{\varepsilon^2} U_* (U_*^2 - 1) - \frac{\mu_0}{\varepsilon^2} - \frac{1}{r} W, \tag{B.1c}$$

$$\mu_0' = 0, \tag{B.1d}$$

$$U_*(r_*) = 1, \quad W(r_*) = 0, \quad S(r_*) = 0 \tag{B.1e}$$

$$W(1) = 0, \quad S(1) = m_0 - \frac{r_*^2}{2}. \tag{B.1f}$$

For an initial choice of $r_* \in (0,1)$ we solve (B.1) except for the condition on $S(1)$ using bvp4c from MATLAB, and then iterate over r_* until the condition on $S(1)$ is satisfied, too. As an initial guess for bvp4c we use

$$S(r) = -\int_0^1 \tanh\left(\frac{r-0.5}{\varepsilon}\right) r dr, \quad U_*(r) = -\tanh\left(\frac{r-0.5}{\varepsilon}\right),$$
$$W(r) = -\frac{1}{\varepsilon}\operatorname{sech}\left(\frac{r-0.5}{\varepsilon}\right)^2, \quad \mu_0(r) = 1,$$

which proved to be sufficient so that the algorithm converges.

Acknowledgments. CP and AM thank Amy Novick-Cohen and Peter Howell for useful discussions.

REFERENCES

[1] H. Abels, H. Garcke, and G. Grün, *Thermodynamically consistent, frame indifferent diffuse interface models for incompressible two-phase flows with different densities*, Math. Models Methods Appl. Sci., 22 (2012), 1150013, https://doi.org/10.1142/S0218202511500138.

[2] H. Abels and M. Wilke, *Convergence to equilibrium for the Cahn–Hilliard equation with a logarithmic free energy*, Nonlinear Anal., 67 (2007), pp. 3176–3193, https://doi.org/10.1016/j.na.2006.10.002.

[3] N. Alikakos, P. Bates, and X. Chen, *Convergence of the Cahn-Hilliard equation to the Hele-Shaw model*, Arch. Ration. Mech. Anal., 128 (1994), pp. 165–205, https://doi.org/10.1007/BF00375025.

[4] R. Almgren, A. Bertozzi, and M. Brenner, *Stable and unstable singularities in the unforced Hele-Shaw cell*, Phys. Fluids, 8 (1996), pp. 1356–1370, https://doi.org/10.1063/1.868915.

[5] G. Barenblatt, E. Beretta, and M. Bertsch, *The problem of the spreading of a liquid film along a solid surface: A new mathematical formulation*, Proc. Natl. Acad. Sci. USA, 94 (1997), pp. 10024–10030, https://www.jstor.org/stable/43152 (accessed 2020-07-24).

[6] J. Barrett and J. Blowey, *Finite element approximation of a degenerate Allen–Cahn/Cahn–Hilliard system*, SIAM J. Numer. Anal., 39 (2002), pp. 1598–1624, https://doi.org/10.1137/S0036142900382144.

[7] J. Barrett, J. Blowey, and H. Garcke, *Finite element approximation of the Cahn–Hilliard equation with degenerate mobility*, SIAM J. Numer. Anal., 37 (1999), pp. 286–318, https://doi.org/10.1137/S0036142997331669.

[8] J. Barrett, H. Garcke, and R. Nürnberg, *A phase field model for the electromigration of intergranular voids*, Interfaces Free Bound., 9 (2007), pp. 171–210, https://doi.org/10.4171/IFB/161.

[9] J. Barrett, R. Nürnberg, and V. Styles, *Finite element approximation of a phase field model for void electromigration*, SIAM J. Numer. Anal., 42 (2004), pp. 738–772, https://doi.org/10.1137/S0036142902413421.

[10] E. Beretta, M. Bertsch, and R. Dal Passo, *Nonnegative solutions of a fourth-order nonlinear degenerate parabolic equation*, Arch. Ration. Mech. Anal., 129 (1995), pp. 175–200, https://doi.org/10.1007/BF00379920.

[11] F. Bernis and A. Friedman, *Higher order nonlinear degenerate parabolic equations*, J. Differential Equations, 83 (1990), pp. 179–206, https://doi.org/10.1016/0022-0396(90)90074-Y.
[12] A. Bertozzi, *Symmetric singularity formation in lubrication-type equations for interface motion*, SIAM J. Appl. Math., 56 (1996), pp. 681–714, https://doi.org/10.1137/S0036139994271972.
[13] A. Bertozzi, *The mathematics of moving contact lines in thin liquid films*, Notices Amer. Math. Soc., 45 (1998), pp. 689–697, http://www.ams.org/notices/199806/bertozzi.pdf (accessed 2013-09-08).
[14] A. Bertozzi, M. Brenner, T. Dupont, and L. Kadanoff, *Singularities and similarities in interface flows*, in Trends and Perspectives in Applied Mathematics, Appl. Math. Sci. 100, Springer, New York, 1994, pp. 155–208, https://doi.org/10.1007/978-1-4612-0859-4_6.
[15] A. Bertozzi and M. Pugh, *The lubrication approximation for thin viscous films: The moving contact line with a porous media cut-off of van der Waals interactions*, Nonlinearity, 7 (1994), pp. 1535–1564, https://doi.org/10.1088/0951-7715/7/6/002.
[16] A. Bertozzi and M. Pugh, *Long-wave instabilities and saturation in thin film equations*, Comm. Pure Appl. Math., 6 (1998), pp. 625–661.
[17] D. Bhate, A. Kumar, and A. Bower, *Diffuse interface model for electromigration and stress voiding*, J. Appl. Phys., 87 (2000), pp. 1712–1721, https://doi.org/10.1063/1.372082.
[18] S. Boatto, L. Kadanoff, and P. Olla, *Traveling-wave solutions to thin-film equations*, Phys. Rev. E, 48 (1993), pp. 4423–4431, https://doi.org/10.1103/PhysRevE.48.4423.
[19] F. Boyer and C. Lapuerta, *Study of a three component Cahn-Hilliard flow model*, ESAIM Math. Model. Numer. Anal., 40 (2006), pp. 653–687, https://doi.org/10.1051/m2an:2006028.
[20] J. Cahn, *On spinodal decomposition*, Acta Metallurgica, 9 (1961), pp. 795–801, https://doi.org/10.1016/0001-6160(61)90182-1.
[21] J. Cahn, *Phase separation by spinodal decomposition in isotropic systems*, J. Chem. Phys., 42 (1965), pp. 93–99, https://doi.org/10.1063/1.1695731.
[22] J. Cahn, C. Elliott, and A. Novick-Cohen, *The Cahn-Hilliard equation with a concentration dependent mobility: Motion by minus the Laplacian of the mean curvature*, European J. Appl. Math., 7 (1996), pp. 287–301, https://doi.org/10.1017/S0956792500002369.
[23] J. Cahn and J. Hilliard, *Free energy of a nonuniform system.* I. *Interfacial free energy*, J. Chem. Phys., 28 (1958), pp. 258–267, https://doi.org/10.1063/1.1744102.
[24] J. Cahn and J. Hilliard, *Spinodal decomposition: A reprise*, Acta Metallurgica, 19 (1971), pp. 151–161, https://doi.org/10.1016/0001-6160(71)90127-1.
[25] J. Cahn and J. Taylor, *Surface motion by surface diffusion*, Acta Metallurgica Materialia, 42 (1994), pp. 1045–1063, https://doi.org/10.1016/0956-7151(94)90123-6.
[26] C. Castellano and S. Glotzer, *On the mechanism of pinning in phase-separating polymer blends*, J. Chem. Phys., 103 (1995), pp. 9363–9369, https://doi.org/10.1063/1.469996.
[27] P. Constantin, T. Dupont, R. Goldstein, L. Kadanoff, M. Shelley, and S.-M. Zhou, *Droplet breakup in a model of the Hele-Shaw cell*, Phys. Rev. E, 47 (1993), pp. 4169–4181, https://doi.org/10.1103/PhysRevE.47.4169.
[28] P. Constantin, T. Elgindi, H. Nguyen, and V. Vicol, *On singularity formation in a Hele-Shaw model*, Comm. Math. Phys., 363 (2018), pp. 139–171, https://doi.org/10.1007/s00220-018-3241-6.
[29] V. Cristini, X. Li, J. Lowengrub, and S. Wise, *Nonlinear simulations of solid tumor growth using a mixture model: Invasion and branching*, J. Math. Biol., 58 (2009), 723, https://doi.org/10.1007/s00285-008-0215-x.
[30] S. Dai and Q. Du, *Motion of interfaces governed by the Cahn–Hilliard equation with highly disparate diffusion mobility*, SIAM J. Appl. Math., 72 (2012), pp. 1818–1841, https://doi.org/10.1137/120862582.
[31] S. Dai and Q. Du, *Coarsening mechanism for systems governed by the Cahn–Hilliard equation with degenerate diffusion mobility*, Multiscale Model. Simul., 12 (2014), pp. 1870–1889, https://doi.org/10.1137/140952387.
[32] S. Dai and Q. Du, *Weak solutions for the Cahn–Hilliard equation with degenerate mobility*, Arch. Ration. Mech. Anal., 219 (2015), pp. 1161–1184, https://doi.org/10.1007/s00205-015-0918-2.
[33] S. Dai and Q. Du, *Computational studies of coarsening rates for the Cahn–Hilliard equation with phase-dependent diffusion mobility*, J. Comput. Phys., 310 (2016), pp. 85–108, https://doi.org/10.1016/j.jcp.2016.01.018.
[34] R. Dal Passo, L. Giacomelli, and A. Novick-Cohen, *Existence for an Allen-Cahn/Cahn-Hilliard system with degenerate mobility*, Interfaces Free Bound., 1 (1999), pp. 199–226, https://doi.org/10.4171/IFB/9.

[35] P. De Gennes, *Dynamics of fluctuations and spinodal decomposition in polymer blends*, J. Chem. Phys., 72 (1980), pp. 4756–4763, https://doi.org/10.1063/1.439809.
[36] H. Ding, P. Spelt, and C. Shu, *Diffuse interface model for incompressible two-phase flows with large density ratios*, J. Comput. Phys., 226 (2007), pp. 2078–2095, https://doi.org/10.1016/j.jcp.2007.06.028.
[37] M. Dziwnik, A. Münch, and B. Wagner, *An anisotropic phase-field model for solid-state dewetting and its sharp-interface limit*, Nonlinearity, 30 (2017), 1465, https://doi.org/10.1088/1361-6544/aa5e5d.
[38] C. Elliott and H. Garcke, *On the Cahn–Hilliard equation with degenerate mobility*, SIAM J. Math. Anal., 27 (1996), pp. 404–423, https://doi.org/10.1137/S0036141094267662.
[39] T. Erneux and S. Davis, *Nonlinear rupture of free films*, Phys. Fluids A, 5 (1993), pp. 1117–1122, https://doi.org/10.1063/1.858597.
[40] V. Galaktionov, *Very singular solutions for thin film equations with absorption*, Stud. Appl. Math., 1 (2010), pp. 39–63.
[41] E. Gawlinski, J. Vials, and J. Gunton, *Domain growth and scaling in the two-dimensional Langevin model*, Phys. Rev. B, 39 (1989), pp. 7266–7269, https://doi.org/10.1103/PhysRevB.39.7266.
[42] K. Glasner, *A diffuse interface approach to Hele–Shaw flow*, Nonlinearity, 16 (2003), 49, https://doi.org/10.1088/0951-7715/16/1/304.
[43] H. Greenspan, *On the motion of a small viscous droplet that wets a surface*, J. Fluid Mech., 84 (1978), pp. 125–143, https://doi.org/10.1017/S0022112078000075.
[44] G. Grün and M. Rumpf, *Nonnegativity preserving convergent schemes for the thin film equation*, Numer. Math., 87 (2000), pp. 113–152, https://doi.org/10.1007/s002110000197.
[45] L. Hocking, *The spreading of a thin drop by gravity and capillarity*, Quart. J. Mech. Appl. Math., 36 (1983), pp. 55–69, https://doi.org/10.1093/qjmam/36.1.55.
[46] B. Hosseini, S. Turek, M. Möller, and C. Palmes, *Isogeometric analysis of the Navier–Stokes–Cahn–Hilliard equations with application to incompressible two-phase flows*, J. Comput. Phys., 348 (2017), pp. 171–194, https://doi.org/10.1016/j.jcp.2017.07.029.
[47] H. Ji and T. Witelski, *Finite-time thin film rupture driven by modified evaporative loss*, Phys. D, 342 (2017), pp. 1–15, https://doi.org/10.1016/j.physd.2016.10.002.
[48] J. King, *Emerging areas of mathematical modelling*, Philos. Trans. A, 358 (2000), pp. 3–19, https://doi.org/10.1098/rsta.2000.0516.
[49] J. King and M. Bowen, *Moving boundary problems and non-uniqueness for the thin film equation*, European J. Appl. Math., 12 (2001), pp. 321–356, https://doi.org/10.1017/S0956792501004405.
[50] A. Lacey, *The motion with slip of a thin viscous droplet over a solid-surface*, Stud. Appl. Math., 67 (1982), pp. 217–230, https://doi.org/10.1002/sapm1982673217.
[51] A. Lee, A. Münch, and E. Süli, *Degenerate mobilities in phase field models are insufficient to capture surface diffusion*, Appl. Phys. Lett., 107 (2015), 081603, https://doi.org/10.1063/1.4929696.
[52] A. Lee, A. Münch, and E. Süli, *Response to "Comment on 'Degenerate Mobilities in phase field models are insufficient to capture surface diffusion'"* [Appl. Phys. Lett. 108, 036101 (2016)], Appl. Phys. Lett., 108 (2016), 036102, https://doi.org/10.1063/1.4939931.
[53] A. Lee, A. Münch, and E. Süli, *Sharp-interface limits of the Cahn–Hilliard equation with degenerate mobility*, SIAM J. Appl. Math., 76 (2016), pp. 433–456, https://doi.org/10.1137/140960189.
[54] E. Lima, J. Oden, B. Wohlmuth, A. Shahmoradi, D. Hormuth, T. Yankeelov, L. Scarabosio, and T. Horger, *Selection and validation of predictive models of radiation effects on tumor growth based on noninvasive imaging data*, Comput. Methods Appl. Mech. Engrg., 327 (2017), pp. 277–305, https://doi.org/10.1016/j.cma.2017.08.009.
[55] H.-W. Lu, K. Glasner, A. Bertozzi, and C.-J. Kim, *A diffuse-interface model for electrowetting drops in a Hele-Shaw cell*, J. Fluid Mech., 590 (2007), https://doi.org/10.1017/S0022112007008154.
[56] M. Mahadevan and R. Bradley, *Phase field model of surface electromigration in single crystal metal thin films*, J. Phys. D, 126 (1999), pp. 201–213, https://doi.org/https://doi.org/10.1016/S0167-2789(98)00276-0.
[57] K. McGuire, A. Laxminarayan, and D. Lloyd, *Kinetics of droplet growth in liquid—liquid phase separation of polymer—diluent systems: Experimental results*, Polymer, 36 (1995), pp. 4951–4960, https://doi.org/10.1016/0032-3861(96)81620-X.
[58] E. Meca, A. Münch, and B. Wagner, *Localized instabilities and spinodal decomposition in driven systems in the presence of elasticity*, Phys. Rev. E, 97 (2018), 012801, https://doi.org/10.1103/PhysRevE.97.012801.

[59] A. Münch and B. Wagner, *Numerical and asymptotic results on the linear stability of a thin film spreading down a slope of small inclination*, European J. Appl. Math., 10 (1999), pp. 297–318, https://doi.org/10.1017/S0956792599003769.

[60] B. Niethammer, *Existence and uniqueness of radially symmetric stationary points within the gradient theory of phase transitions*, European J. Appl. Math., 6 (1995), https://doi.org/10.1017/S0956792500001662.

[61] A. Novick-Cohen and A. Shishkov, *The thin film equation with backwards second order diffusion*, Interfaces Free Bound., 12 (2011), pp. 463–496, https://doi.org/10.4171/IFB/242.

[62] J. Oden, E. Lima, R. Almeida, Y. Feng, M. Rylander, D. Fuentes, D. Faghihi, M. Rahman, M. DeWitt, M. Gadde, and J. Zhou, *Toward predictive multiscale modeling of vascular tumor growth: Computational and experimental oncology for tumor prediction*, Arch. Comput. Methods Engrg., 23 (2015), pp. 735–779, https://doi.org/10.1007/s11831-015-9156-x.

[63] R. Pego, *Front migration in the nonlinear Cahn-Hilliard equation*, Proc. A, 422 (1989), pp. 261–278, https://doi.org/10.1098/rspa.1989.0027.

[64] D. Peschka, A. Münch, and B. Niethammer, *Self-similar rupture of viscous thin films in the strong-slip regime*, Nonlinearity, 23 (2010), pp. 409–427, https://doi.org/10.1088/0951-7715/23/2/010.

[65] D. Peschka, A. Münch, and B. Niethammer, *Thin-film rupture for large slip*, J. Engrg. Math., 66 (2010), pp. 33–51, https://doi.org/10.1007/s10665-009-9342-7.

[66] A. Rätz, A. Ribalta, and A. Voigt, *Surface evolution of elastically stressed films under deposition by a diffuse interface model*, J. Comput. Phys., 214 (2006), pp. 187–208, https://doi.org/10.1016/j.jcp.2005.09.013.

[67] T. Rogers, K. Elder, and R. Desai, *Numerical study of the late stages of spinodal decomposition*, Phys. Rev. B, 37 (1988), pp. 9638–9649, https://doi.org/10.1103/PhysRevB.37.9638.

[68] P. Rybka and K.-H. Hoffmann, *Convergence of solutions to Cahn-Hilliard equation*, Comm. Partial Differential Equations, 24 (1998), pp. 1055–1077, https://doi.org/https://doi.org/10.1080/03605309908821458.

[69] D. Sibley, A. Nold, and S. Kalliadasis, *Unifying binary fluid diffuse-interface models in the sharp-interface limit*, J. Fluid Mech., 736 (2013), pp. 5–43, https://doi.org/10.1017/jfm.2013.521.

[70] J. Taylor and J. Cahn, *Linking anisotropic sharp and diffuse surface motion laws via gradient flows*, J. Stat. Phys., 77 (1994), pp. 183–197, https://doi.org/10.1007/BF02186838.

[71] S. Torabi and J. Lowengrub, *Simulating interfacial anisotropy in thin-film growth using an extended Cahn–Hilliard model*, Phys. Rev. E, 72 (2012), https://doi.org/https://doi.org/10.1103/PhysRevE.85.041603.

[72] S. Torabi, J. Lowengrub, A. Voigt, and S. Wise, *A new phase-field model for strongly anisotropic systems*, Proc. A, 465 (2009), pp. 1337–1359, https://doi.org/10.1098/rspa.2008.0385.

[73] S. van Gemmert, G. Barkema, and S. Puri, *Phase separation driven by surface diffusion: A Monte Carlo study*, Phys. Rev. E, 72 (2005), https://doi.org/https://doi.org/10.1103/physreve.72.046131.

[74] D. Vaynblat, J. Lister, and T. Witelski, *Rupture of thin viscous films by van der Waals forces: Evolution and self-similarity*, Phys. Fluids, 13 (2001), pp. 1130–1140, https://doi.org/doi:10.1063/1.1359749.

[75] D. Vaynblat, J. Lister, and T. Witelski, *Symmetry and self-similarity in rupture and pinchoff: A geometric bifurcation*, European J. Appl. Math., 12 (2001), https://doi.org/10.1017/S0956792501004375.

[76] A. Voigt, *Comment on "Degenerate mobilities in phase field models are insufficient to capture surface diffusion"* [Appl. Phys. Lett. 107, 081603 (2015)], Appl. Phys. Lett., 108 (2016), 036101, https://doi.org/10.1063/1.4939930.

[77] T. Witelski and A. Bernoff, *Dynamics of three-dimensional thin film rupture*, Phys. D, 147 (2000), pp. 155–176, https://doi.org/10.1016/S0167-2789(00)00165-2.

[78] J. K. Wolterink, G. T. Barkema, and S. Puri, *Spinodal decomposition via surface diffusion in polymer mixtures*, Phys. Rev. E, 74 (2006), 011804, https://doi.org/10.1103/PhysRevE.74.011804.

[79] L. Zhornitskaya and A. Bertozzi, *Positivity-preserving numerical schemes for lubrication-type equations*, SIAM J. Numer. Anal., 37 (2000), pp. 523–555, https://doi.org/https://doi.org/10.1137/S0036142998335698.